Research Article | Vol. 12, No. 3 / 1 March 2021 / Biomedical Optics Express 1295
Biomedical Optics EXPRESS

Dielectric property measurements of corneal tissues for computational dosimetry of the eye in terahertz band *in vivo* and *in vitro*

MAYA MIZUNO,[1,*] HIDEAKI KITAHARA,[2] KENSUKE SASAKI,[1] MASAHIKO TANI,[2] MASAMI KOJIMA,[3] YUKIHISA SUZUKI,[4] TAKAFUMI TASAKI,[3,5] YOSHINORI TATEMATSU,[2] MASAFUMI FUKUNARI,[2] AND KANAKO WAKE[1]

[1]*National Institute of Information and Communications Technology, Koganei, Tokyo 184-8795, Japan*
[2]*Research Center for Development of Far-Infrared Region, University of Fukui, Fukui 910-8507, Japan*
[3]*Medical Research Institute, Kanazawa Medical University, Kahoku, Ishikawa 920-0293, Japan*
[4]*Graduate School of Systems Design, Tokyo Metropolitan University, Hachioji, Tokyo 192-0397, Japan*
[5]*Department of Medical Zoology, Kanazawa Medical University, Kahoku, Ishikawa 920-0293, Japan*
[*]*mmizuno@nict.go.jp*

Abstract: The dielectric constant of the normal corneal tissue of a rabbit eye was obtained *in vitro* in the range from approximately 0.1 to 1 THz, and the drying process on the eye surface exposed to high-power terahertz waves was investigated by *in vivo* reflectance measurement using terahertz time-domain spectroscopy. When the rabbit eye was exposed to terahertz waves at 162 GHz for 6 min with an irradiation power of 360 or 480 mW/cm^2, the reflectance temporally increased and then decreased with a temperature increase. Based on multiple-reflection calculation using the dielectric constant and anterior segment optical coherence tomography images, those changes in reflectance were attributed to drying of the tear and epithelium of the cornea, respectively. Furthermore, the drying progressed over a temperature increase of around 5°C under our exposure conditions. These findings suggest that the possibility of eye damage increases with the progress of drying and that the setting of the eye surface conditions can be a cause of disagreement between computational and experimental data of absorbed energy under high-level irradiation because reflectance is related to terahertz wave penetration in the eye tissue. The time-domain spectroscopic measurements were useful for the acquisition of the dielectric constant as well as for the real-time monitoring of the eye conditions during exposure measurement.

1. Introduction

Terahertz (THz) wave applications such as nondestructive testing [1], wireless communication [2], and biological sensing are now feasible. The frequency range from 252 to 325 GHz has been considered for wireless communication in IEEE 802.15.3d [3], and peripheral techniques have been developed. A study on the wireless power transfer technique in the THz band [4] was also conducted. In the medical field, technologies for examining burn wounds [5] or corneal tissue water content [6] have been developed. Such testing of surface tissues has become possible owing to the development of THz measurement systems [7–9]. For these practical uses, it is necessary to study the interactions between THz waves and cells or tissues such as the skin and eyes to investigate the possible effects of THz waves on human health. Both nonthermal and thermal effects in this frequency region have been investigated [10–12]. For example, as thermal effect investigations, evaluation of the level of irradiation to tissues, calculation of the temperature elevation in tissues [13], and investigation of the exposure threshold for tissue damage are required [14]. Moreover, the investigated data should be physically and visually analyzed in detail by

#412769 https://doi.org/10.1364/BOE.412769
Journal © 2021 Received 23 Oct 2020; revised 16 Jan 2021; accepted 27 Jan 2021; published 8 Feb 2021

Biomedical Optics EXPRESS

computational dosimetry using the dielectric constants of biological substances [15]. To perform precise dosimetry evaluation, real information on the changes in the dielectric constant, and thus, the reflection and absorption properties during an exposure measurement, is necessary because these properties are related to THz wave penetration into the tissue.

In this paper, we report the THz spectroscopic measurement results of corneal tissues to clarify the dielectric properties and eye surface conditions during the exposure measurement. These results were required for the computational dosimetry of the eye in our recent investigation on the exposure damage threshold for 162 GHz irradiation [16]. The frequency is in a characteristic range from approximately 100 GHz to 200 GHz, in which the real and imaginary parts of the dielectric constant have similar values. Investigation in this frequency range is an important step toward the next physical investigation and exposure measurement in the 300 GHz band. We measured the complex dielectric constants of the normal cornea of rabbits in the THz range from approximately 0.1 to 1 THz, taking individual deviations into account. Since, for computational dosimetry, it is important to know the transient change in the dielectric properties of substances, we also monitored the changes in reflectance from the surface of the cornea during exposure to the THz waves with relatively high power of 360 or 480 mW/cm^2 *in vivo*. In our previous paper [16], we reported that these power levels affected most, if not all, rabbit eye specimens. In this study, these power levels were used to clarify the physical cause of the eye damage. To our best knowledge, this is the first noninvasive measurement of the real-time change in the dielectric properties of rabbit corneas during exposure to electromagnetic waves in the frequency band. The collaborative technologies of the high-power THz source, THz spectroscopy, and exposure measurement enabled transient dielectric property acquisition for the computational dosimetry of the eye in the THz band. The results indicate that the dielectric property at the exposed position markedly changes under high-power THz irradiation, and it is necessary to take into account the transient changes in the eye surface conditions for the reliable computational dosimetry of the eye.

2. Measurement specimens and systems

2.1. Spectrometers

To evaluate the complex dielectric constant of the cornea, several different types of spectrometer were used. Broadband spectra were measured using a 1 mm coaxial sensor in the frequency range from 1 to 100 GHz and an attenuated total reflection (ATR)-type THz time-domain spectroscopy (TDS) system (TAS7500TS, ADVANTEST Co.) in the frequency range from 100 GHz to 3 THz. The coaxial sensor was connected to a millimeter-wave test head module (N5260, Agilent Technologies) with a network analyzer (E8361, Agilent Technologies) [17,18]. To cover the ATR measurement frequency range, two types of THz emitter were used: a bowtie-type photoconductive antenna (PCA) and a dipole-type PCA. A temperature controller (thermoplate, Tokai Hit Co., Ltd., or glass heater, BLAST Inc.) was used to heat the tissue specimens to maintain the temperature at approximately 35°C; each specimen was sandwiched between a silicon ATR prism and the temperature controller, as shown in Fig. 1(a). We also used a transmission (T)-type THz-TDS system for measurements at frequencies from 100 GHz to 1 THz. The T-type THz-TDS system consisted of a parallel THz beam system and a temperature controller with a Peltier device. To suppress the influence of the curvature of the specimen and moisture evaporation, the specimen was sandwiched between two quartz plates and then heated to approximately 33°C by the temperature controller [Fig. 1(b)].

To monitor reflectance, a reflection (R)-type THz-TDS system [T-Ray 4000, Picometrix LLC (currently Luna Innovations Inc.)] was used. This system can be set up with vertical or oblique incidence of the THz beam, as shown in Figs. 1(c) and 1(d), respectively. The reflectance measurements were carried out with a focal optical system consisting of one or two lenses made of white polyethylene. The focal lengths of the lenses were 1 and 6 inches for vertical and oblique

Biomedical Optics EXPRESS

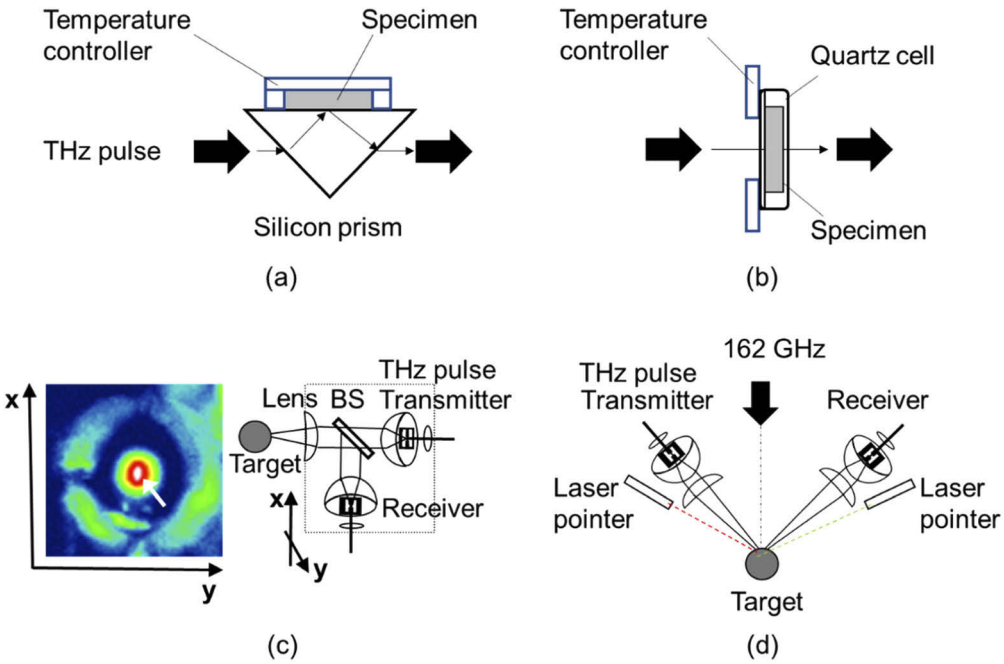

Fig. 1. Schematic diagram of the setups of specimens for (a) ATR and (b) T-type dielectric constant measurement, and reflectance measurement systems for (c) vertical and (d) oblique incidences. The white arrow in the left x-y image of (c) indicates the position with the largest reflection signal.

(45°) incidences, respectively. In the vertical incidence type, a two-dimensional reflection signal of a target was acquired using an x-y stage, and then the reflectance was calculated using the signal at the position with the largest reflection and a reference signal from a metal ball. In the oblique incidence type, the target was set at the position for 162 GHz exposure, as indicated by two laser pointers mentioned later, and then the angles of the target were adjusted to obtain a maximum reflection signal before a monitoring measurement. The polarizations of THz pulses for the R-type THz-TDS system and the 162 GHz wave were set to be vertical. The THz-TDS measurement is helpful for distinguishing the changes in reflectance caused by, for example, eye condition and movement.

2.2. Corneal specimens and experimental animals

For the measurement of the dielectric constant, we used normal porcine and rabbit corneas separated from eye tissues cooled to a low temperature or from experimental animals used for the THz exposure measurements mentioned later. The porcine and rabbit eye tissues used for ATR-type THz-TDS measurement were purchased from Tokyoshibaurazouki Co., Ltd., and Funakoshi Co., Ltd., Japan, respectively. The latter specimens were used for T-type THz-TDS measurement within 20 min of corneal tissue acquisition. The center thickness of rabbit corneas was measured *in vivo* using an optical coherence tomography (OCT) system (Model 5000, Zeiss, Japan). Rabbits were used for the *in vivo* exposure experiment. The animal experiments were conducted in accordance with animal study guidelines [14] and approved by the Animal Research Committee of the University of Fukui. The rabbits (*Oryctolagus cuniculus*; strain, Kbt:Dutch; male) were purchased from Sankyo Labo Service Co., Inc. (Toyama, Japan) and kept at the Research Center for Development of Far-Infrared Region, University of Fukui [19].

Biomedical Optics EXPRESS

They were fed 170 g of laboratory-grade chow (Labo R Stock, Nosan, Japan) once daily and tap water was given without restriction. Medetomidine hydrochloride (0.5 mg/kg body weight, subcutaneous injection: Domitor, Nippon Zenyaku Kogyo Co., Ltd., Japan) and buprenorphine hydrochloride (0.05 mg/kg, intramuscular injection: Buprenorphine, Nippon Shinyaku Co., Ltd., Japan) were administered to the rabbits to induce anesthesia and analgesia. Before the exposure experiment, the anesthetized rabbits were immobilized in an acrylic restrainer and the rabbit eyes were examined using a slit-lamp microscope to ensure the absence of abnormalities in the anterior segment. Immediately before the exposure to THz waves, 2% lidocaine hydrochloride, a topical anesthetic, was administered to each eye. The upper and lower eyelids were held open with tape. Because anesthesia suppressed blinking, saline drops, prewarmed to 35–37 °C, were administered to the eyes as necessary to prevent damage to corneal epithelial cells resulting from corneal desiccation. Temperature and humidity during exposure were maintained at 24 ± 2°C and 60 ± 10%, respectively, using an air conditioner and a humidifier. After the experiment, the rabbits were euthanized by an intravenous administration of pentobarbital sodium (81 mg/kg, Somnopentyl, Kyoritsu Seiyaku Corporation, Japan) to dissect the rabbit corneas from the eyes. For dielectric constant and vertical reflection measurements, aqueous solutions on the rabbit cornea surface were removed using a sponge absorber for medical treatment before each measurement. The preparation and analysis of the rabbit corneal tissues, as shown in Fig. 2, were carried out in the same building, so that we could maintain the same specimen conditions for all procedures.

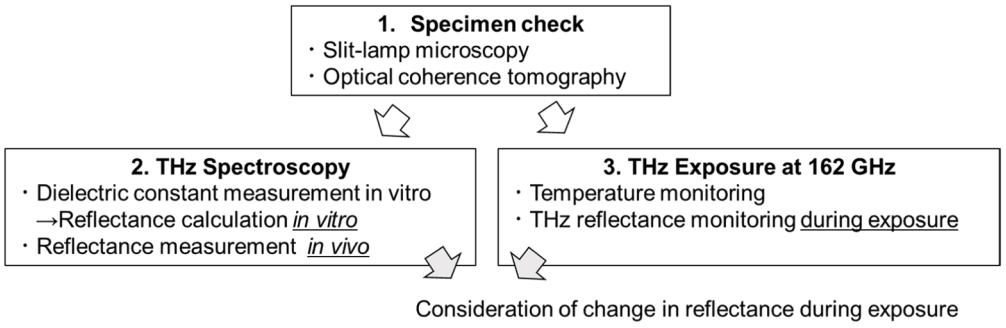

Fig. 2. Schematic diagram of analysis using rabbit corneal specimens.

2.3. THz exposure system

To monitor the change in reflectance during the THz exposure, a THz exposure system consisting of a THz gyrotron (Gyrotron FU CW GV [20]) was operated at 162 GHz with a duty ratio of 99.9999%. The THz beam was focused to the surface of the rabbit cornea using a lens antenna with a diameter of 100 mm and a focal length of 200 mm. A schematic diagram of the developed exposure system is shown in Fig. 3. The focused beam area defined with $1/e^2$ intensity decay was approximately 1.41 cm^2. Incident power of 318, 478, or 637 mW was used. The Gaussian power distribution was verified using a waveguide probe (AOEWGP-02/3.0, Elmika) with the gain obtained by the three-antenna method [21] and a power meter (Erikson PM4, Virginia Diodes Inc.) [16], and then the total power incident to the lens antenna was monitored using a power meter (Erikson PM5, Virginia Diodes Inc.). Here, the spatially averaged power per area with a diameter of 13.0 mm, which is the average size of the corneal region in Dutch-belted rabbits, was calculated as 240, 360, or 480 mW/cm^2. These values are called power densities in this paper. Note that the beam power density was approximately 227, 341, or 455 mW/cm^2. The exposure point was set by adopting a procedure with red and green laser pointers [13] to ensure

Biomedical Optics EXPRESS

fine reproducibility of the *in vivo* experiments. The THz exposure time was set to 6 min so that we can understand the relation with the 6 min average power density in the international guidelines developed by International Commission on Non-Ionizing Radiation Protection [22] and Japanese radio-radiation protection guidelines for human exposure to electromagnetic fields [23]. During the exposure measurement, corneal surface temperatures were recorded at a 30 Hz sampling rate using a thermography camera (FLIR T620, FLIR Systems, Oregon, USA).

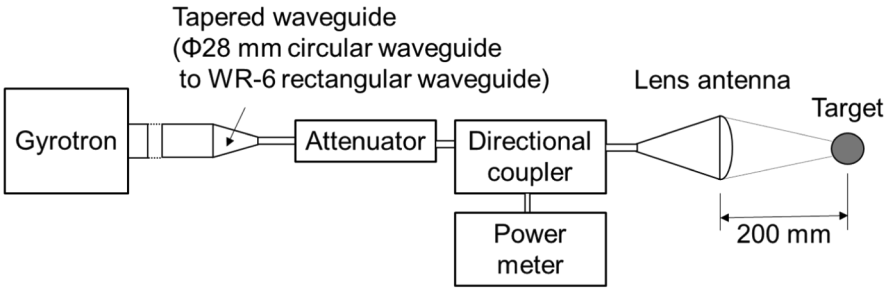

Fig. 3. Schematic diagram of the developed 162 GHz exposure system.

3. Measurement results and discussion

3.1. Dielectric constant measurements

We first measured the dielectric constants of porcine and rabbit normal corneas at approximately 35°C in the frequency range from 1 GHz to 3 THz using the 1 mm coaxial sensor and the ATR-type TDS system. In addition, the dielectric constants of saline were measured for comparison because we know that corneal tissue is over 70% water. In Fig. 4, the means of four measurement data are plotted. We confirmed that the magnitudes of saline dielectric constants were larger than those of the corneas, and the dielectric loss peak frequencies of the corneas were shifted to a slightly lower frequency from that of the saline, as shown in the inset of Fig. 4, with error bars indicating sample standard deviations. The frequency shift was approximately 4 GHz. These differences indicate that the motion of water molecules inside the tissue was disturbed. A similar shift was also confirmed in a previous paper [17]. From these results, it is concluded that the dielectric constant of tear fluid, which is close to that of saline, is larger than that of the corneal tissue at frequencies under 220 GHz. If a corneal tissue is completely covered with tear fluid or saline, an increase in reflectance will be observed. The difference in the dielectric characteristic is mainly caused by water content [24], which is the dominant factor causing individual deviations.

To evaluate individual deviations among specimens, we measured the dielectric constants of four rabbit corneas in the range from 0.1 to 1 THz using the T-type THz-TDS system. We used specimens with storage time shorter than those used in the case of Fig. 4. The cornea thickness was confirmed *in vivo* to be 0.36, 0.37, 0.37, or 0.36 mm in the center position using the OCT system. When we measured the dielectric constant, the specimens were placed in a quartz cell for 0.3 mm specimen thickness. The mass densities of the sandwiched specimens might therefore be nonuniform because the cornea thickness slightly differed between the center and the edges. Figure 5 shows the sample means of the dielectric constant of rabbit cornea. Here, multiple-reflection influences were removed by the zero filling method. Error bars indicate three times the sample standard deviation for the T-type measurement. Although variation could be observed, the spectral tendencies agreed among the four specimens. Moreover, the real part in the ATR-type measurement was within three times the sample standard deviation for the T-type measurement, even though the imaginary part was slightly larger in the T-type measurement than in the ATR-type measurement at higher frequencies. The spectra could be fitted by the

Biomedical Optics EXPRESS

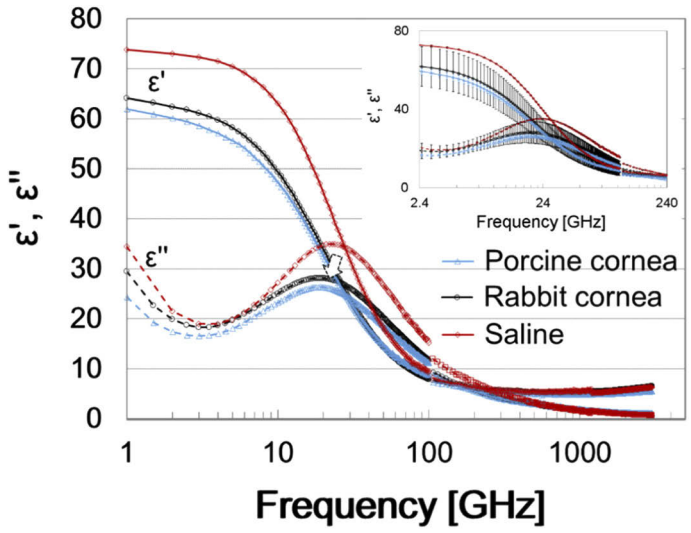

Fig. 4. Dielectric constants of rabbit corneal specimen (black circles), porcine corneal specimen (blue triangles), and saline (red diamonds) at approximately 35°C in the frequency range from 1 GHz to 3 THz (real part: solid; imaginary part: broken). An arrow marks the difference in the dielectric loss peak between saline and cornea. The inset indicates the sample standard deviations of the data at around the peak frequency.

double Debye model, as in the case of the water spectrum [25]. From the fitting, the real and imaginary parts of the dielectric constant were found to be 6.0 and 7.2, respectively, at around 162 GHz. From these values, the reflectance and absorption coefficient were calculated as 30% and 88 cm^{-1}, respectively. To confirm that the data obtained *in vitro* were valid, we compared the calculated reflectance with measured reflectance data obtained *in vivo* [Fig. 6(b)]. *In vivo* measurements were carried out using the R-type THz-TDS system with vertical incidence of the THz beam, as shown in Fig. 1(c) and Fig. 6(a). A two-dimensional reflection signal of each eye was acquired using an x-y stage, and then the reflectance was calculated from the signal at the position with the largest reflection (near the center of the eye) and a reference signal from an aluminum ball of 20 mm diameter. A material with curvature similar to the eye was needed because different curvature caused a small reflectance at low frequencies with large beams owing to the decrease in the magnitude of the THz signal reflected toward the detector. We used two rabbits, and both the left and right eyes were used for the measurements. The four data were almost the same, except for random fluctuations. Thus, the inter-subject variation was small. The reflectance data was in fair agreement within three times the sample standard deviation in the low-frequency region under 0.3 THz. We considered that the dielectric loss differed between the corneal epithelium and the stroma, or the THz beam path was optically changed inside the corneal specimen, and the detection loss on the PCA of the T-type THz-TDS system increased at higher frequencies. Such data variations would be observed if the sample thickness were slightly nonuniform [26]. Despite these possibilities, our data were reliable at frequencies under 0.3 THz.

3.2. *Reflectance and temperature monitoring*

Using the R-type THz-TDS operating at a center frequency of approximately 0.3 THz with oblique incidence, as shown in Fig. 1(d) and Fig. 7(a), we verified the possibility of a change in reflectance during the exposure measurement. Beforehand, we verified the reflectance difference between the eyes before and after exposure to THz waves at 162 GHz. In the measurement, a power density of 240 mW/cm^2 was used. We placed the rabbit eye near the target position, and

Biomedical Optics EXPRESS

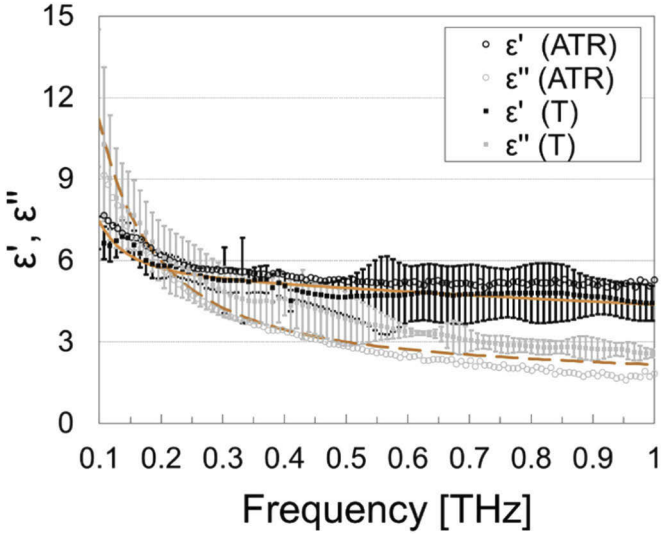

Fig. 5. Dielectric constant of rabbit corneal specimen at frequencies from 0.1 to 1 THz measured using ATR-type (circles) or T-type (squares) THz-TDS (real part: black; imaginary part: gray). We fitted the double Debye model to the data (real part: orange solid; imaginary part: orange broken).

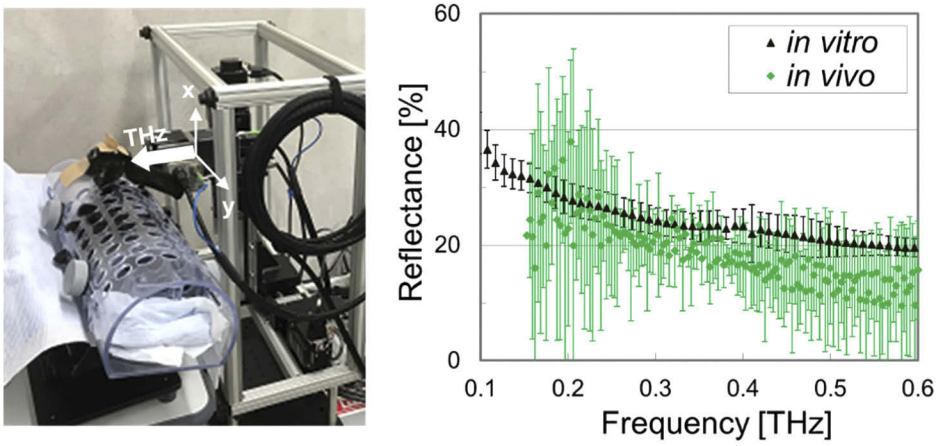

Fig. 6. (a) Photograph of reflectance measurement setup and (b) reflectance spectra of corneal tissue *in vitro* (brown triangles) and *in vivo* (green diamonds). Three times the sample standard deviation of the four measurements is indicated.

Biomedical Optics EXPRESS

adjusted the eye to the best position where the THz pulse electric field reflected from the rabbit eye surface was the largest. Immediately before each measurement, surplus water was removed by a sponge absorber. The THz electric fields were monitored for 180 s, and then the average change in reflectance ratio (R/R_0) was calculated from the amplitude of the negative peak in the THz waveform because the measured THz waveforms had larger negative peaks than positive ones. Here, R_0 is the reflectance at 0 s without the exposure. The graph in Fig. 7(b) and its inset show the calculated average changes in reflectance and examples of the reflected THz pulse electric field in the time domain at 0, 100, 157, and 170 s, respectively, which were obtained without the exposure. When the irradiation power was 0 mW/cm^2, the ratios were almost 100% even though large eye motions while trying to blink sometimes caused erroneous changes in reflectance as a result of distortion of the THz pulse waveform, such as those observed at around 157 s. After the exposure, the reflectance ratio became approximately 40%. In addition, the THz time-domain waveforms were sometimes shifted, for example, at 100 and 170 s, as shown in the inset of Fig. 7(b), probably owing to small eye motions. The shifts were approximately 1.6 ps, corresponding to a 0.35 mm shift in the 162 GHz beam propagation direction. This shift was much smaller than the Rayleigh length of the 162 GHz beam. Thus, the change in the irradiation beam power density caused by the shift can be ignored. These results showed the possibility of detecting the changes in reflectance in the eye for each power density in real time.

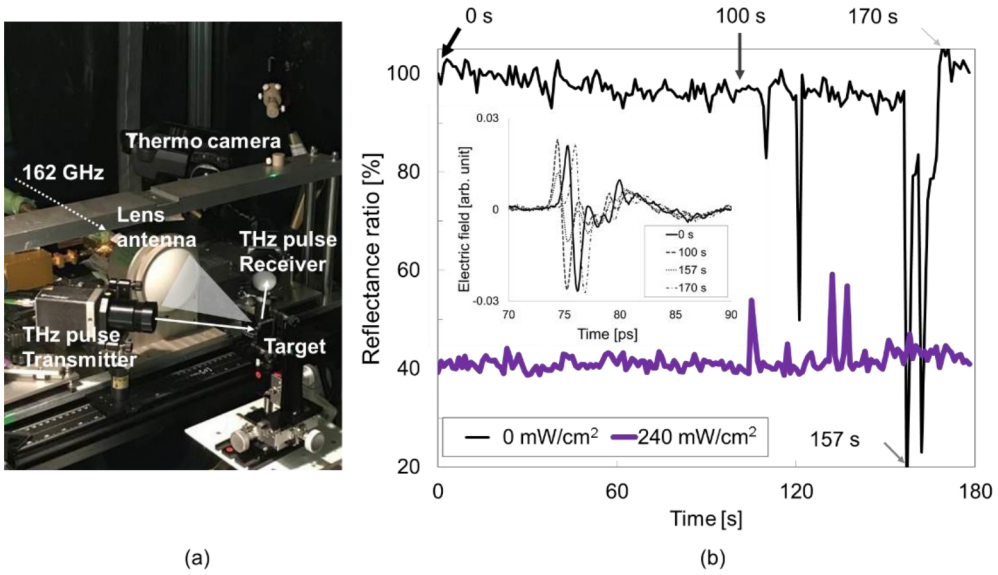

Fig. 7. (a) Photograph of exposure equipment and spectroscopy system and (b) average changes in reflectance of rabbit eye surface after THz exposure to 0 (thinner line) and 240 mW/cm^2 (thicker line). The inset shows examples of the reflected THz pulse electric field in the time domain at 0, 100, 157, and 170 s for the case of no exposure.

We attempted real-time monitoring with exposure to two different high power densities of 360 and 480 mW/cm^2, which were expected to induce a large difference in the tendency of reflectance changes. The measurement point was identified on a target by the red and green laser pointers mentioned above. The temperature of the eye surface was also measured using the thermography camera. Figure 8 shows examples of the changes in temperature (upper figure) and reflectance ratio R/R_0 (lower figure) for about 570 s with 360 and 480 mW/cm^2 exposures. In Fig. 8, vertical dotted lines indicate the start and finish of exposure. The horizontal dashed line indicates a 100%

Biomedical Optics EXPRESS

reflectance ratio (no difference from R at 0 s, R_0). When irradiation started, the reflectance ratio from the eye surface slightly increased, and then decreased with a rapid temperature increase, as shown in Fig. 8. The total increases in temperature were approximately 13 and 15°C for 360 and 480 mW/cm^2 exposures, respectively. Generally, the dielectric constant (or reflectance) of water increases with increasing temperature at around 0.3 THz [25]. However, other tendencies were also observed. For example, there was a temporal increase in the reflectance ratio at around 160 s. In addition, the reflectance increased while the temperature rapidly decreased after the end of exposure at 480 mW/cm^2. Tear overflow on or penetrating into part of the cornea may have caused the change in reflectance. Furthermore, the time shift of the THz pulse peak (change in beam path) owing to eye movements frequently caused the signal to decrease. For exposure of 360 mW/cm^2, many time shift effects were observed after 78 s. Multiple phenomena that could have caused the signal changes are included in Fig. 8.

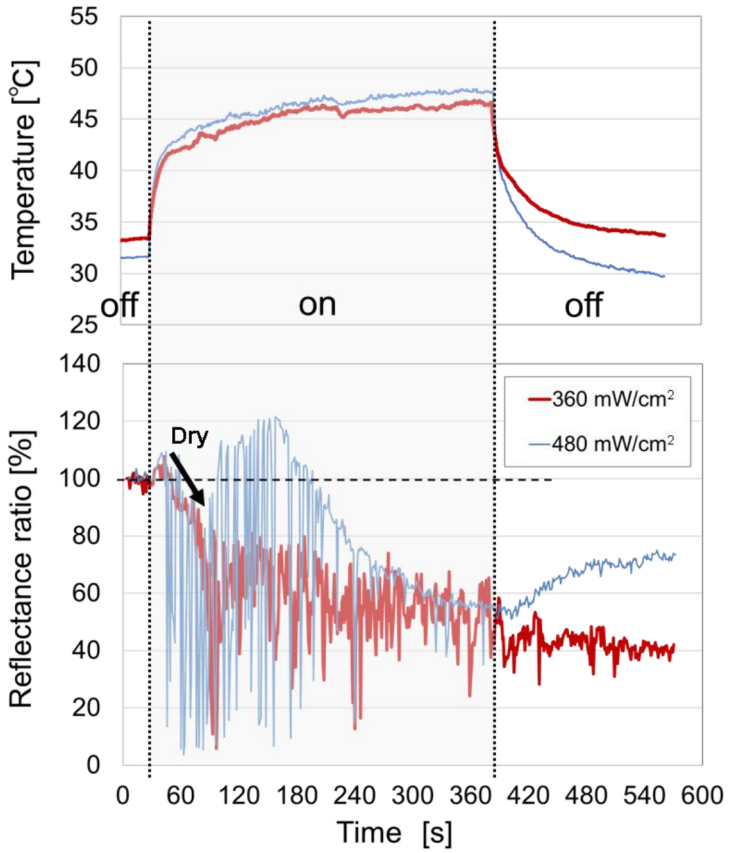

Fig. 8. Time course of temperature and THz reflectance ratio on rabbit eye surface. The data were acquired for 30 s before, for 6 min during, and for 3 min after exposure to a THz wave of 360 (red) or 480 mW/cm^2 (blue).

To remove the changes due to eye movement and determine the approximate drying temperature, we plot the relationship between the temperature change and the reflectance ratio during the temperature increase in Fig. 9, using the data within a THz pulse peak shift range of ±0.5 ps. In this range, most of the control specimens had reflectance data of over 95% as shown in the inset of Fig. 9. Here the reflectance at the start of measurement was used as R_0. As the temperature

Biomedical Optics EXPRESS

data, the means of the temperature changes of four rabbit corneas were plotted for each exposure condition. The error bars indicate three times the sample standard deviation of the temperature data of four rabbit corneas. As shown in this graph, the changes in the reflectance ratio for both exposure conditions were in reasonable qualitative agreement. The reflectance ratio was almost constant until the temperature increase of around 5°C, and then slightly increased. After the increase, the reflectance ratio decreased. We verified that the temperature dependence of the dielectric constant was not the only cause of the change in reflectance. If the fluid layer on the eye (including the anesthesia and saline used before each measurement) dries, the fluid layer thickness and the refractive index of the tear film consisting of water and mucin will decrease. After the fluid layer dries, the water content inside the cornea will decrease. These occurrences affect the THz reflectance.

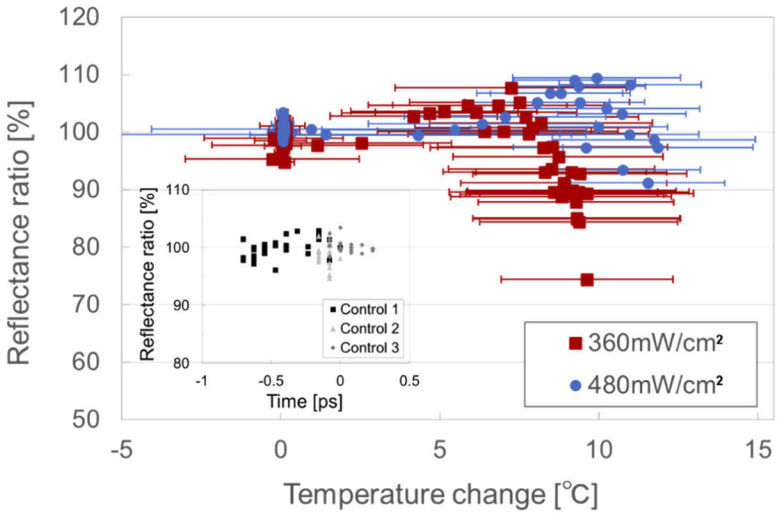

Fig. 9. Relationship between temperature change and THz reflectance ratio on rabbit eye surface. Red squares and blue circles are data for 360 and 480 mW/cm^2 exposures, respectively. Error bars indicate three times the sample standard deviation of the temperature data of four rabbit corneas.

3.3. Discussion of drying process

To verify the changes in the reflectance owing to the occurrences mentioned above, we calculated the reflectance ratio using an approximate model comprising three dielectric layers of air, saline, and cornea, whose dielectric constants at 0.3 THz were used. The Fresnel equations used in the calculation are as follows.

$$r_s = (n_s \cos\theta_a - \cos\theta_s)/(n_s \cos\theta_a + \cos\theta_s)) \tag{1}$$

$$r_c = (n_c \cos\theta_s - n_s \cos\theta_c)/(n_c \cos\theta_s + n_s \cos\theta_c)) \tag{2}$$

$$R = \left\{ r_s + \sqrt{1-(r_s)^2}\sqrt{T_s} r_c \cos(4\pi n_s d \cos\theta_s/\lambda) \right\}^2 \tag{3}$$

Subscripts a, s, and c indicate air, saline, and cornea, respectively. The Fresnel reflection coefficient r was calculated from the refractive index at a wavelength λ of 1 mm, the incidence angle, and the refraction angle on each layer. The reflectance R was derived using the reflection coefficients, the supposed thickness d, and the transmittance T_s calculated from the absorption coefficient and propagation distance in the saline layer. The reflection ratio (R/R_0) was calculated

Biomedical Optics EXPRESS

using the reflectance of a 0.005-mm-thick saline layer as R_0. Figure 10 shows the reflectance ratio calculated for saline thicknesses below 0.05 mm. The reflectance ratio became small with decreasing thickness owing to the interference of THz waves reflected from each layer, and the ratio was almost constant at 100% below 0.01 mm. However, because the tear film includes mucin, the refractive index of the tear layer of the eye may decrease with decreasing thickness when the ratio of the amounts of water and mucin decreases. We therefore also show the relationship between the reflectance ratio and the supposed refractive index in the inset of Fig. 10 as an example. The reflectance ratio increased with decreasing refractive index regardless of the relative magnitudes of the refractive indices of the layers. Compared with the measurement results from around 5°C, the tendency of the reflectance ratio to increase agreed. Because the changes in reflectance are related to the changes in THz wave penetration into the eye tissues, these data suggest that the computational data of absorbed energy with a constant dielectric property can be the cause of disagreement with its experimental data in the case of high-power exposure.

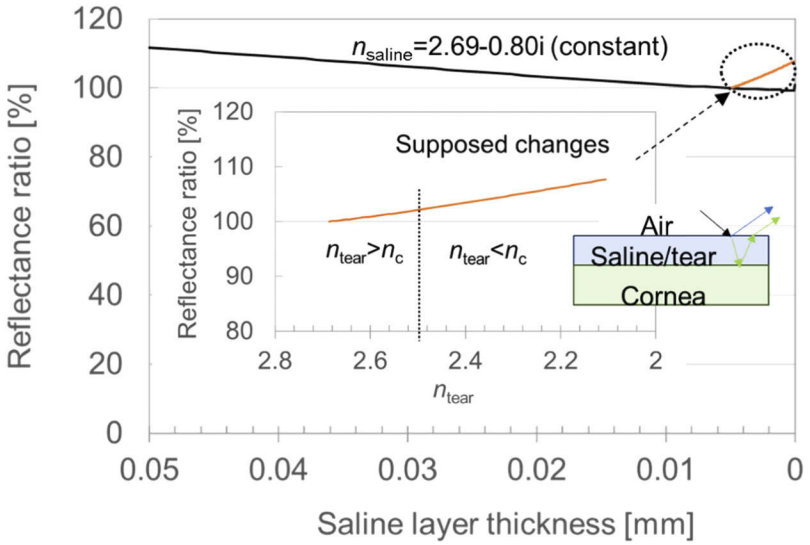

Fig. 10. Relationship between the THz reflectance ratio and the thickness of the saline layer calculated using the approximate model comprising three layers with air, saline (or tear), and cornea. The inset indicates the relationship between the THz reflectance ratio and the supposed refractive index of the tear layer below 0.005 mm.

In addition, we considered that as the temperature change increased, the tear fluid dried even if it was periodically added, and then the water content inside the cornea decreased. Anterior segment OCT images taken before and one day after exposure are shown in Fig. 11. The corneal edema seen after THz exposure convexified on the corneal epithelium side. The corneal edema is thought to be due to the entry of water into the corneal stroma from the site of the corneal epithelium defect caused by the induced cell death. Thus, it was clarified that the corneal epithelium side was mainly heated and dried by the THz exposure. Also, in our previous study [16] we observed that corneal epithelial cell damage was large when the maximum temperature was above 41°C. Furthermore, the thickness of the cornea reversibly decreased immediately after the exposure with 480 mW/cm^2. These clinical results support our consideration. The acute drying caused by 162 GHz exposure can be a trigger for corneal epithelium damage.

Biomedical Optics EXPRESS

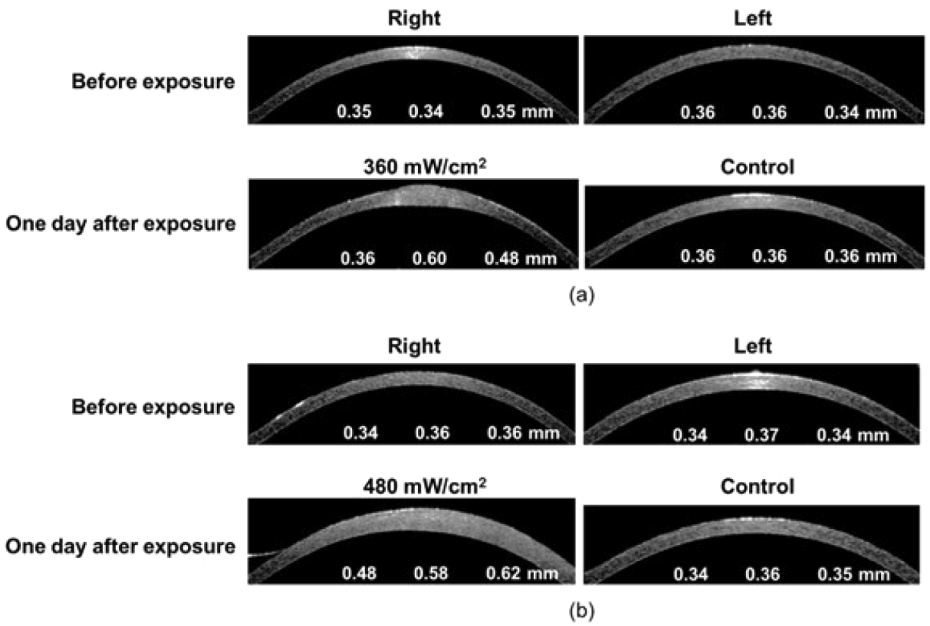

Fig. 11. Anterior segment OCT images of rabbit eyes before and one day after exposure of (a) 360 and (b) 480 mW/cm^2. Right eyes were exposed to each power density and left eyes were the control. The thicknesses of the cornea at the center, 1.5 mm to the left of the center, and 1.5 mm to the right of the center are indicated.

4. Summary

The dielectric constant of the normal corneal tissue of rabbit eye at body temperature in the THz band was investigated. The dielectric constant was independent of the animal species. However, the tendency of the change in reflection from the corneal surface differed between the control condition and 360 or 480 mW/cm^2 exposure; the dielectric constant was changed at the same position during exposure measurement. Increase in reflectance from temperature increase of 5°C was mainly caused by decreases in the refractive index owing to drying of the eye surface. The decrease in reflectance with increasing temperature change was related to drying in the corneal epithelium. Because the reflectance is related to the penetration of the THz wave into the eye tissues, the changes in the dielectric constant and the drying of the surface layer during exposure are suggested to be key information in physically analyzing the possibility of eye damage by simulating the THz wave energy absorbed by the eye tissue. Also, discussion of the blink frequency and the environmental humidity, which are directly related to the dryness of the cornea, will be important in a general environment. The results showed that time-domain measurement can provide data supporting the computational dosimetry of the eye in the THz band.

Funding. Ministry of Internal Affairs and Communications (JPMI10001).

Acknowledgments. The authors thank Dr. Soichi Watanabe and Dr. Masao Taki of National Institute of Information and Communications Technology for their valuable suggestions.

Disclosures. The authors declare that there are no conflicts of interest related to this article.

References

1. I. Amenabar, F. Lopez, and A. Mendikute, "In introductory review to THz non-destructive testing of composite mater," J. Infrared, Millimeter, Terahertz Waves **34**(2), 152–169 (2013).
2. J. Federici and L. Moeller, "Review of terahertz and subterahertz wireless communications," J. Appl. Phys. **107**(11), 111101 (2010).

Biomedical Optics EXPRESS

3. . IEEE Std 802.15.3d-2017, *IEEE Standard for High Data Rate Wireless Multi-media Networks*, Amendment 2: 100 Gb/s wireless switched point-to-point physical layer (IEEE, 2017).
4. S. Mizojiri, K. Shimamura, M. Fukunari, S. Minakawa, S. Yokota, Y. Yamaguchi, Y. Tatematsu, and T. Saito, "Subterahertz wireless power transmission using 303-GHz rectenna and 300-kW-class gyrotron," IEEE Microwave Wireless Compon. Lett. **28**(9), 834–836 (2018).
5. M. H. Arbab, T. C. Dickey, D. P. Winebrenner, A. Chen, M. B. Klein, and P. D. Mourad, "Terahertz reflectometry of burn wounds in a rat model," Biomed. Opt. Express **2**(8), 2339–2347 (2011).
6. Z. D. Taylor, J. Garritano, S. Sung, N. Bajwa, D. B. Bennett, B. Nowroozi, P. Tewari, J. W. Sayre, J.-P. Hubschman, S. X. Deng, E. R. Brown, and W. S. Grundfest, "THz and mm-wave sensing of corneal tissue water content: *in vivo* sensing and imaging results," IEEE Trans. Terahertz Sci. Technol. **5**(2), 184–196 (2015).
7. G. J. Wilmink, B. L. Ibey, T. Tongue, B. Schulkin, N. Laman, X. G. Peralta, C. C. Roth, C. Z. Cerna, B. D. Rivest, J. E. Grundt, and W. P. Roach, "Development of a compact terahertz time-domain spectrometer for the measurement of the optical properties of biological tissues," J. Biomed. Opt. **16**(4), 047006 (2011).
8. S. Sung, S. Selvin, N. Bajwa, S. Chantra, B. Nowroozi, J. Garritano, J. Goell, A. D. Li, S. X. Deng, E. R. Brown, W. S. Grundfest, and Z. D. Taylor, "THz imaging system for *in vivo* human cornea," IEEE Trans. Terahertz Sci. Technol. **8**(1), 27–37 (2018).
9. S. Sung, S. Dabironezare, N. Llombart, S. Selvin, N. Bajwa, S. Chantra, B. Nowroozi, J. Garritano, J. Goell, A. Li, S. X. Deng, E. Brown, W. S. Grundfest, and Z. D. Taylor, "Optical system design for noncontact, normal incidence, THz imaging of *in vivo* human cornea," IEEE Trans. Terahertz Sci. Technol. **8**(1), 1–12 (2018).
10. G. J. Wilmink and J. E. Grundt, "Invited review article: current state of research on biological effects of terahertz radiation," J. Infrared, Millimeter, Terahertz Waves **32**(10), 1074–1122 (2011).
11. M. R. Scarfì, M. Romanò, R. Di Pietro, O. Zeni, A. Doria, G. P. Gallerano, E. Giovenale, G. Messina, A. Lai, G. Campurra, D. Coniglio, and M. D'Arienzo, "THz exposure of whole blood for the study of biological effects on human lymphocytes," J. Biol. Phys. **29**(2/3), 171–176 (2003).
12. B. S. Alexandrov, M. L. Phipps, L. B. Alexandrov, L. G. Booshehri, A. Erat, J. Zabolotny, C. H. Mielke, H.-T. Chen, G. Rodriguez, KØ Rasmussen, J. S. Martinez, A. R. Bishop, and A. Usheva, "Specificity and heterogeneity of terahertz radiation effect on gene expression in mouse mesenchymal stem cells," Sci. Rep. **3**(1), 1184 (2013).
13. M. Kojima, Y. Suzuki, C.-Y. Tsai, K. Sasaki, K. Wake, S. Watanabe, M. Taki, Y. Kamimura, A. Hirata, K. Sasaki, and H. Sasaki, "Characteristics of ocular temperature elevations after exposure to quasi- and millimeter waves (18–40 GHz)," J. Infrared, Millimeter, Terahertz Waves **36**(4), 390–399 (2015).
14. M. Kojima, Y. Suzuki, K. Sasaki, M. Taki, K. Wake, S. Watanabe, M. Mizuno, T. Tasaki, and H. Sasaki, "Ocular effects of exposure to 40, 75, and 95 GHz millimeter waves," J. Infrared, Millimeter, Terahertz Waves **39**(9), 912–925 (2018).
15. K. Sasaki, M. Mizuno, K. Wake, and S. Watanabe, "Monte Carlo simulations of skin exposure to electromagnetic field from 10 GHz to 1 THz," Phys. Med. Biol. **62**(17), 6993–7010 (2017).
16. M. Kojima, Y. Suzuki, T. Tasaki, Y. Tatematsu, M. Mizuno, M. Fukunari, and H. Sasaki, "Clinical course of high-frequency millimeter-wave (162 GHz) induced ocular injuries and investigation of damage thresholds," J. Infrared, Millimeter, Terahertz Waves **41**(7), 834–845 (2020).
17. K. Sasaki, Y. Ishimura, K. Fujii, K. Wake, S. Watanabe, M. Kojima, R. Suga, and O. Hashimoto, "Dielectric property measurement of ocular tissues up to 110 GHz using 1 mm coaxial sensor," Phys. Med. Biol. **60**(16), 6273–6288 (2015).
18. K. Sasaki, A. Nishikata, S. Watanabe, and O. Fujiwara, "Intercomparison of methods for measurement of dielectric properties of biological tissues with a coaxial sensor at millimeter-wave frequencies," Phys. Med. Biol. **63**(20), 205008 (2018).
19. T. Tasaki, M. Kojima, Y. Suzuki, Y. Tatematsu, and H. Sasaki, "Creating a stable short-term housing environment for rabbits in a cargo van," J. Am. Assoc. Lab. Anim. Sci. **58**(4), 456–461 (2019).
20. Y. Tatematsu, Y. Yamaguchi, R. Ichioka, M. Kotera, T. Saito, and T. Idehara, "Development of the multifrequency gyrotron FU CW GV with Gaussian beam output," J. Infrared, Millimeter, Terahertz Waves **36**(8), 697–708 (2015).
21. K. Harima, "Numerical simulation of far-field gain determination at reduced distances using phase center," IEICE Trans. Commun. **E97.B**(10), 2001–2010 (2014).
22. International Commission on Non-Ionizing Radiation Protection, "Guidelines for limiting exposure to time-varying electric, magnetic, and electromagnetic fields (up to 300 GHz)," Health Phys. **74**(4), 494–522 (1998).
23. Telecommunications Technology Council, "Radio-Radiation Protection Guidelines for Human Exposure to Electromagnetic Fields," Report No. 89 (1997).
24. D. Bennett, Z. Taylor, P. Tewari, S. Sung, A. Maccabi, R. Singh, M. Culjat, W. Grundfest, J. P. Hubschman, and E. Brown, "Assessment of corneal hydration sensing in the terahertz band: in vivo results at 100 GHz," J. Biomed. Opt. **17**(9), 0970081 (2012).
25. C. Rønne, L. Thrane, P.-O. Åstrand, A. Wallqvist, K. V. Mikkelsen, and S. R. Keiding, "Investigation of the temperature dependence of dielectric relaxation in liquid water by THz reflection spectroscopy and molecular dynamics simulation," J. Chem. Phys. **107**(14), 5319–5331 (1997).
26. M. Mizuno, H. Iida, M. Kinoshita, K. Fukunaga, Y. Shimada, and C. Otani, "Classification of terahertz spectrometer for transmittance measurements of refractive materials," IEICE Electron. Express **13**(18), 20160532 (2016).